Sunflower hard disk graphs

Carl P. Dettmann[1] and Orestis Georgiou[2,1]

[1]School of Mathematics, University of Bristol, United Kingdom
[2]Ultraleap Ltd, Bristol, United Kingdom

May 16, 2023

Abstract

The random geometric graph consists of a random point set with links between points with mutual distance below a fixed threshold. Here, we use the same geometric connection rule ("hard disk graph") but for a deterministic point set, the sunflower spiral. At large distances, the local structure is asymptotically a lattice where for each lattice vector, there is another of length a factor $\sqrt{5}$ greater, and the angle between these varies log-periodically with distance from the origin. Graph properties including node degrees, stretch factor, clique and chromatic numbers are considered, as well as link formation, connectivity and planarity transitions. Properties depend on a combination of the central region and the perturbed distant lattices, in a rich and varied manner.

Keywords: Hard disk graphs, network structure, spatial networks, sunflower spiral

1 Introduction

A geometric graph, or spatial network, consists of a set of points ("nodes") located in a metric space (typically $\mathbb{R}^2$), together with a set of links between pairs of nodes. Geometric graphs are used to model, for example, social, transport, wireless and neuronal networks, in which nodes represent respectively people, places, cellphones and neurons [Bar11]. In each of these, links are more likely between close pairs of nodes. One very simple class of models called hard disk graphs is to link pairs of nodes with a mutual distance less than or equal to a fixed threshold R. We could (without loss of generality) take $R = 1$ (and use the term "unit disk") and instead scale the point set or metric by R^{-1}, however it is often more natural to keep the point set fixed, and vary R, and focus attention on the combinatorial graph formed by the nodes and links. The combinatorial properties discussed in such systems includes degrees, connectivity, planarity and chromatic number, and are well known and discussed below; an accessible introduction is found in Ref. [Est15]. Further, there is a plethora of other connectivity functions (deterministic and stochastic) that can be used to form links between nodes [Det16].

One very popular hard disk model is the random geometric graph [Wal11], in which the nodes are randomly distributed, and links are formed according to the hard disk rule. For example, consider a domain $\mathcal{D} \subset \mathbb{R}^2$ of area $|\mathcal{D}|$ and smooth boundary; the prototypical example in the literature is the unit square domain. The usual meaning of "randomly distributed" is a Poisson point process [Las18] of constant density λ in $\mathcal{D}$. Then, the mean number of nodes is $\bar{N} = \lambda|\mathcal{D}|$ and the mean degree (number of nodes linked to any given node) is $\bar{D} = \lambda\pi R^2$, ignoring boundary effects. The graph properties are random due to the node locations, but taking a limit in which $\bar{N} \to \infty$ and R (and hence $\bar{D}$) varies in a specified manner leads to sharp transitions, that is, change of properties that have probability approaching unity in the limit. Two well studied transitions are percolation, the existence of a connected cluster of size proportional to $\bar{N}$, when $\bar{D}$ exceeds a critical constant (known to be close to 4.51 in this model), and connectivity, all nodes being contained in a single connected cluster, when $\bar{D} - \ln \bar{N} \to \infty$ [Wal11]. There is a large literature on this and related models in probability [Pen16], statistical physics [Spe18], wireless communications [Det18] and the spatial networks mentioned above.

It is also possible to apply the hard disk connection rule to deterministic point sets. Lattice models used in statistical physics are an example of this, where each node is connected to its nearest neighbours, or in addition, its next nearest neighbours, and so on. However, in this case, the network properties (degree distribution, etc) are often trivial. One example of a nontrivial deterministic hard disk graph is that of low-discrepancy sequences considered in Ref. [Est17]. In this case, many properties are similar to the random geometric graph, especially for larger connection radius, but the degree distributions are more concentrated.

In this paper, we will explore properties of the hard disk graph of a single deterministic point set, the *sunflower spiral*, and will unveil an extremely rich and interesting combinatorial structure despite its very simple definition. The name of this point set arises from its use in modelling the pattern of sunflower seeds and
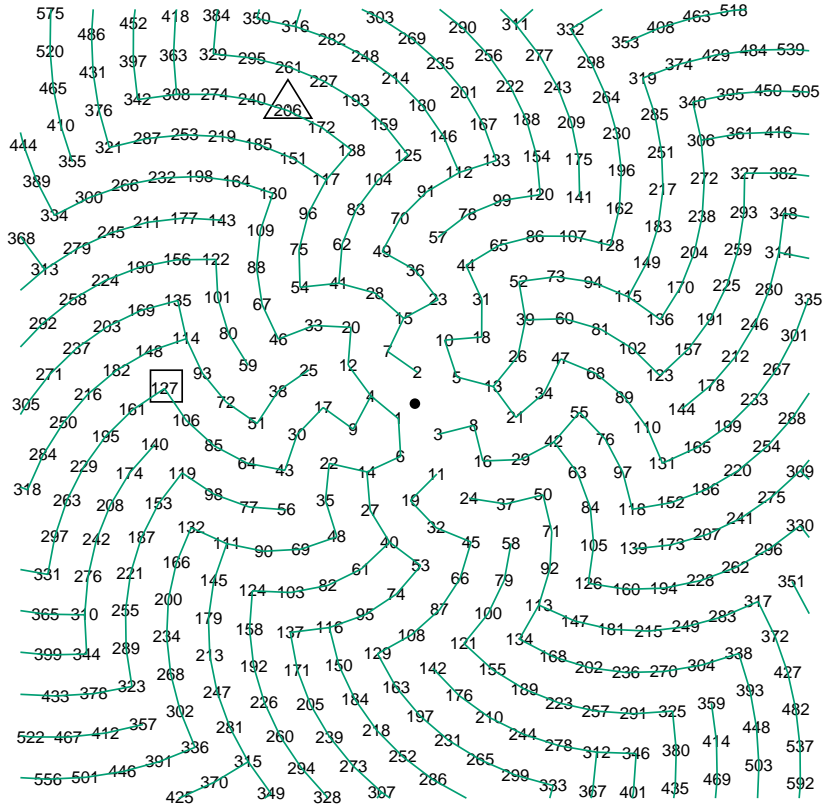
Figure 1: Sunflower graph with $R = 1$, for $x, y \in [-10, 10]$ and the origin $(k = 0)$ marked with a dot. The point locations (x, y) and numbers k are defined in Eq. 1. The points 127 and 206 are examples of the square and isosceles lattice locations discussed in Sec. 3 and following.

similar biological systems; see Refs. [Vog79, Mac21]. It consists of a discrete set of points located on a spiral with polar equation of the form $r = c\sqrt{\phi}$ with $c > 0$ first studied by Fermat in 1636 [Law13]; other terms used for this and related sets in the literature are Vogel and Fermat spirals, and spiral lattices. The discrete set is usually chosen with equal spacing using the golden angle $(3 - \sqrt{5})\pi = (2 - g)2\pi \approx 137.5°$ where $g = (1 + \sqrt{5})/2 \approx 1.618$ is the golden ratio. A similar pattern has also been obtained using a physics experiment with drops of ferrofluid [Dou92]. Despite the discrete nature of the set, it exhibits a highly uniform density and circular symmetry which make it of interest in technological applications, for example in reducing side lobes in a transducer array [Pri18], light confinement in quantum photonic devices [Tro21] and for directional light emission [Gor18], situating mirrors in concentrated solar energy generation plants [Bar16] and designing rib-reinforced shell structures [Men23]. Even a small deviation from the golden angle leads to very different structure [Tre12].

Recent mathematical work includes proofs that this and related point sets satisfy the Delone property [Aki20, Mar20] (discussed below), including in a nonstandard metric [Yam20] and have Voronoi cells with area converging at large distances [Yam21]. Visibility properties of spiral sets were considered in Ref. [Adi22b].

In the following sections, we consider the hard disk graph on the sunflower spiral

(see for example Fig. 1) and present an exploratory study of this simply defined yet remarkably rich system. For each graph property we consider, the result depends on either the region near the origin, or the log-periodically varying lattice far from the origin, often switching between these in a complicated manner as a function of the connection range R. Even for the distant lattices, the properties at the transition points, and more non-local properties (degrees for large connection radius, and chromatic number) depend sensitively on the nature of the small perturbations of these lattices, that is, their deviation from exact lattices, decreasing with distance from the origin.

The paper is structured as follows: In Sec. 2 we define the sunflower spiral and explain why each point's neighbours have label differing from it by Fibonacci numbers. In Secs. 3 and 4 we consider the lattice structure far from the origin, and show that it oscillates between the square lattice and a lattice of isosceles triangles. In Sec. 5 we discuss Delone properties and spanning ratio. In Sec. 6 we consider transitions in which new classes of links are formed as R is varied, mostly at the isosceles lattices, and also connectivity and planarity. In Sec. 7 we investigate minimum and maximum degrees, which involve either near nodes or the distant lattices and observe a number of interesting phenomena. In Sec. 8 we consider the harder problems of clique and chromatic numbers. Finally the conclusion in Sec. 9 outlines many possible future directions.

2 The sunflower spiral and Fibonacci numbers

Let $g = \frac{1+\sqrt{5}}{2} \approx 1.618$ be the golden ratio, satisfying $g^2 = g + 1$. We define the sunflower spiral $S \subset \mathbb{R}^2$ using polar coordinates as [Vog79]

$$
\begin{aligned}
S &= \{(x_k, y_k) : k = 1, 2, 3, \ldots\} \\
x_k &= r_k \cos \phi_k, \qquad y_k = r_k \sin \phi_k, \\
r_k &= \sqrt{\frac{k}{\pi}}, \qquad \phi_k = 2\pi k g.
\end{aligned}
\tag{1}
$$

The number of points in a radius r of the origin is πr^2, so the average density is unity; it turns out that the points are quite uniformly distributed [Aki20, Yam21]. We will usually refer to a point by the label k rather than the Cartesian or polar coordinates. The Euclidean distance between two points j and k will be denoted by $d_{j,k}$.

Looking at Fig. 1, we make a key observation:

> **Closely spaced points have values of k differing by Fibonacci numbers.**

The Fibonacci numbers $1, 1, 2, 3, 5, 8, 13, 21, 34, 55, 89, \ldots$ are defined by $F_1 = F_2 = 1$, $F_n = F_{n-1} + F_{n-2}$. We can explain this for large k as follows, though it is true even close to the origin. Consider a point k. A point j will be close to k, meaning that $d_{j,k}$ is of order unity, if both these conditions are met:

(a) The radial distance is order unity or less.

(b) The tangential distance is order unity or less.

For condition (a), the radial distance between nearby points k and j is

$$|r_j - r_k| = \frac{1}{\sqrt{\pi}} \left| \sqrt{j} - \sqrt{k} \right| = \frac{1}{\sqrt{\pi}} \frac{|j - k|}{\sqrt{j} + \sqrt{k}} \tag{2}$$

which is order unity if $|j - k|$ is order $\sqrt{k}$. Thus we need $|j - k| = O(\sqrt{k})$, or equivalently that $j/k = 1 + O(k^{-1/2})$.

For condition (b), the tangential distance is approximately

$$r_k(\phi_j - \phi_k - 2\pi N) = 2\sqrt{\pi k} \left[(j - k)g - N \right] \tag{3}$$

where N is the nearest integer to $(j - k)g$. Thus, we need $\|(j - k)g\| = O(k^{-1/2})$, where $\| \cdot \|$ denotes the distance to the nearest integer.

To make progress we need to calculate $\|mg\|$, where m is an arbitrary integer. Recall that the Fibonacci numbers are known to satisfy

$$F_n = \frac{1}{\sqrt{5}} \left[g^n - (-g)^{-n} \right] \tag{4}$$

which is sometimes called Binet's formula. Comparing adjacent Fibonacci numbers we obtain

$$gF_n = F_{n+1} - (-g)^{-n} \tag{5}$$

and hence that g multiplied by a large Fibonacci number is close to the next Fibonacci number, and also that F_{n+1}/F_n is a close rational approximant for g since g^{-n} is exponentially small for large n. Next, by repeatedly subtracting the largest Fibonacci number less than an arbitrary positive integer m and noting the Fibonacci recursion above, we can write m as a finite sum of non-consecutive F_n with $n \geq 2$,

$$m = \sum_{n=2}^{\infty} a_n F_n \tag{6}$$

with $a_n \in \{0, 1\}$ and $a_n a_{n+1} = 0$. Combining this with Eq. (5) we find

$$mg = \sum_{n=2}^{\infty} a_n \left[F_{n+1} - (-g)^{-n} \right] \tag{7}$$

In this expression the F_{n+1} terms are integers and the powers of $(-g)^{-n}$ sum to at most

$$\sum_{n=1}^{\infty} g^{-2n} = g^{-1} \approx 0.618034 \tag{8}$$

in magnitude. Thus

$$\|mg\| = \left| \sum_{n=2}^{\infty} a_n (-g)^{-n} - c \right| \tag{9}$$

where $c \in \{-1, 0, 1\}$ is the closest integer to the sum.

Returning to condition (b) above, we must have only terms with $g^{-n} = O(k^{-1/2})$. But from Eq. (4) we have that $F_n \sim g^n/\sqrt{5}$. So, $m = |j - k|$ can be written as a sum of non-consecutive Fibonacci numbers at least as large as order $\sqrt{k}$.

Condition (a) requires that $|j - k|$ be at most of order $\sqrt{k}$, whilst condition (b) requires that $|j - k|$ be written as a sum of non-consecutive Fibonacci numbers at least of order $\sqrt{k}$. Combining these, we find that in order to have the distance $d_{j,k}$ of order unity, we need $|j - k|$ to be written as a sum of non-consecutive Fibonacci numbers, all of order $\sqrt{k}$. Finally, to reduce distance in both directions, the closest point must be only a single Fibonacci number F_n, of order $\sqrt{k}$. This last statement is only an intuitive argument, but we provide more precise calculations of the distance in Sec. 4. Also, numerically, the closest point being a Fibonacci difference $|j - k|$ holds for all k, not just large k.

We remark that if g were replaced by another irrational number α, a similar calculation could be made, in which the Fibonacci numbers are replaced by the denominators of its sequence of best rational approximants ("convergents") of α as detailed in Ref. [Roc92], and in terms of which the equation Eq. (6) above is the Ostrowski expansion with respect to α [Ost22, Lek51, Roc92]. There are some recent results for spirals from more general irrationals in Ref. [Aki20].

3   Local structure at large k

As shown in the previous section, the radial and angular displacement of a nearby point j from k depends only on the magnitude of k, to leading order, and on the difference $k - j$ constructed from a few Fibonacci numbers of order $\sqrt{k}$. Also, since the point j is roughly the same order of magnitude as k, it must have a similar neighbourhood given the same differences. Thus, the local structure of the set in the vicinity of k is that of a lattice. To see this, we choose as a basis the two displacement vectors $k \to j = k + F_n$ and $k \to l = k + F_{n+1}$, with n chosen so that F_n is roughly of magnitude $\sqrt{k}$ and gives the closest point to k in the outward direction (this value is given in Eq. (21) below). Other lattice vectors are linear combinations of these, for example, $F_{n-1} = F_{n+1} - F_n$.

We can identify some examples of these local lattices by looking again at Fig. 1. Observe that $k = 127$ (left of centre) is surrounded by an almost square lattice with steps of 21 and 34 in k in orthogonal directions. Close to $k = 206$ (near the top, left of centre), the arrangement is close to an anisotropic triangular lattice with steps of 21, 34 and 55 (all of which are Fibonacci) in the three directions, and the 34 distance slightly smaller. We will later show that the local lattice structure at k oscillates between these two.

Next, we shall make these observations quantitative and establish the local geometry of the lattice as a function of k. Let k be large, and (ξ, η) be the local coordinate system centred at point k and defined by the radial and angular displacements from k respectively. Specifically, we have notation as in Eq. (1),

$$\begin{pmatrix} \xi \\ \eta \end{pmatrix} = \begin{pmatrix} \cos\phi_k & \sin\phi_k \\ -\sin\phi_k & \cos\phi_k \end{pmatrix} \begin{pmatrix} x - x_k \\ y - y_k \end{pmatrix} \tag{10}$$

such that the local coordinate system (ξ, η) has been rotated by ϕ_k and its origin has been translated by (x_k, y_k). Then, for $j = k + F_n$ with F_n of order $\sqrt{k}$, we have that

$$r_j = \sqrt{\frac{k + F_n}{\pi}} = r_k + \frac{F_n}{2\sqrt{\pi k}} + \mathcal{O}(k^{-1/2}) \tag{11}$$

$$\phi_j = \phi_k - 2\pi(-g)^{-n} + 2\pi F_{n+1} \tag{12}$$

using Eq. (5). The final term in Eq. (12) may be neglected since F_{n+1} is an integer. Combining these equations together with Eqs. (4,10) leads to the first basis vector of the local lattice geometry

$$\xi_j = \frac{g^n}{2\sqrt{5\pi k}} + \mathcal{O}(k^{-1/2}) \tag{13}$$

$$\eta_j = -2\sqrt{\pi k}(-g)^{-n} + \mathcal{O}(k^{-1/2}) \tag{14}$$

with g^n also of order $\sqrt{k}$. The second basis vector can be obtained through a similar calculation for the point $l = k + F_{n+1}$. Finally, we can find the area of the parallelogram defined by k, j, l, and $k + F_n + F_{n+1}$ through

$$A = \left| \det \begin{bmatrix} \xi_j & \eta_j \\ \xi_l & \eta_l \end{bmatrix} \right| = 1 + \mathcal{O}(k^{-1/2}) \tag{15}$$

which is independent of k as $k \to \infty$, showing that these define a covolume one lattice as expected. That the area approaches unity in the large k limit has been rigorously proven in Ref. [Yam21].

4 Lattices at large k

Assuming that k is large, in this section we shall neglect the $\mathcal{O}(k^{-1/2})$ terms. We then have that a lattice vector from k to a nearby point $k + aF_n + bF_{n+1}$ for integers a and b (i.e., a linear combination of the two basis vectors) has, from Eqs. (13) and (14), displacement

$$\xi = \frac{g^n}{2\sqrt{5\pi k}} (a + gb) \tag{16}$$

$$\eta = -2\sqrt{\pi k}(-g)^{-n} (a - b/g) \tag{17}$$

Notice that replacing k by $k' = g^2 k$ leads to the same form of equations with $\xi' = \xi$, $\eta' = -\eta$, $a' = b - a$ and $b' = a$ where the latter transformation is invertible. Thus, we can conclude the lattice repeats log-periodically (modulo a trivial reflection) when k is multiplied by g^2 and hence r is multiplied by g. Likewise, it is log-reflection symmetric in that replacing k by $k' = g^{2m}/(80\pi^2 k)$ leads to the same lattice with suitable transformations, now interchanging ξ and η.

The squared distance of the lattice vector in Eqs. (16,17) is $\delta_{a,b}^2 = \xi^2 + \eta^2$. So, the squared lengths of the basis vectors k to $k + F_n$ and k to $k + F_{n+1}$ are

respectively

$$\delta_{1,0}^2 = \frac{1}{\sqrt{5}} \left(\kappa_n + \kappa_n^{-1} \right) \tag{18}$$

$$\delta_{0,1}^2 = \frac{1}{\sqrt{5}} \left(\kappa_n g^{-2} + \kappa_n^{-1} g^2 \right) \tag{19}$$

where

$$\kappa_n = \frac{4\pi\sqrt{5}}{g^{2n}} k \tag{20}$$

Fig. 2 plots all the node distances (vertical axis) as a function of k (horizontal axis, logarithmic scale). The upper panel does this for $1 \leq k \leq 10^6$, using the actual node distances, and illustrates the convergence as k increases to the log-periodic and log-reflection symmetric pattern as derived above. The lower panel shows a single fundamental domain of this pattern in the limit, using the large k approximations implicit in Eqs. (16), (17).

The lines of reflection symmetry, the left and right extremes of the lower panel of Fig. 2 are of particular importance. Namely, at the right extreme, where $k = \frac{g^{2n+1}}{4\pi\sqrt{5}}$ and $\kappa_n = g$, we have the unit square lattice, at which the two basis vectors are of equal length and orthogonal; beyond this $k + F_{n+1}$ is now closer to k than $k + F_n$. Thus we expect $k \pm F_n$ to be the closest point to k when $\frac{g^{2n-1}}{4\pi\sqrt{5}} < k < \frac{g^{2n+1}}{4\pi\sqrt{5}}$, that is, $g^{-1} < \kappa_n < g$, under the large k approximation. Inverting this to write n in terms of k we find

$$n_{min}(k) = \lfloor \frac{\ln(4\pi\sqrt{5}gk)}{2\ln g} \rfloor \tag{21}$$

Numerically, the closest point always differs by a Fibonacci number, even for very small k. In some cases (small k, and near the square lattice) the value of n for the closest point can differ by 1 from the prediction in the above equation.

At the left extreme of the lower panel of Fig. 2, $k = \frac{g^{2n}}{4\pi\sqrt{5}}$ and $\kappa_n = 1$, the distance $\delta_{1,0}$ is minimised, and the distances k to $k + F_{n-1}$ and k to $k + F_{n+1}$, that is, $\delta_{-1,1}$ and $\delta_{0,1}$ respectively, are equal. In this case the lattice consists of isosceles triangles with side lengths $\sqrt{\frac{2}{\sqrt{5}}}, \sqrt{\frac{3}{\sqrt{5}}}, \sqrt{\frac{3}{\sqrt{5}}}$. We denote this the isosceles (triangle) lattice. It can also be described as a centred rectangular lattice, that is, a rectangular lattice with side lengths $\sqrt{\frac{2}{\sqrt{5}}}, \sqrt{2\sqrt{5}}$ together with a point at the centre of each rectangle. Both these lattices are visible in Fig. 1, for example near $k = 127 \approx \frac{g^{17}}{4\pi\sqrt{5}}$ and $k = 206 \approx \frac{g^{18}}{4\pi\sqrt{5}}$ respectively, as noted in the previous section.

Note that a general two dimensional lattice has two parameters, up to scale and orientation, namely the angle and ratio of lengths of the two basis vectors. In the case of the sunflower spiral point set S however, we have a family of lattices with only a single parameter determined by k. Thus, there must be an additional condition yet to be satisfied in order to describe the lattice structure of S. It is not difficult to check that for any k and any (a, b), we have

$$\delta_{-a+2b,2a+b}^2 = 5\delta_{a,b}^2 \tag{22}$$

8
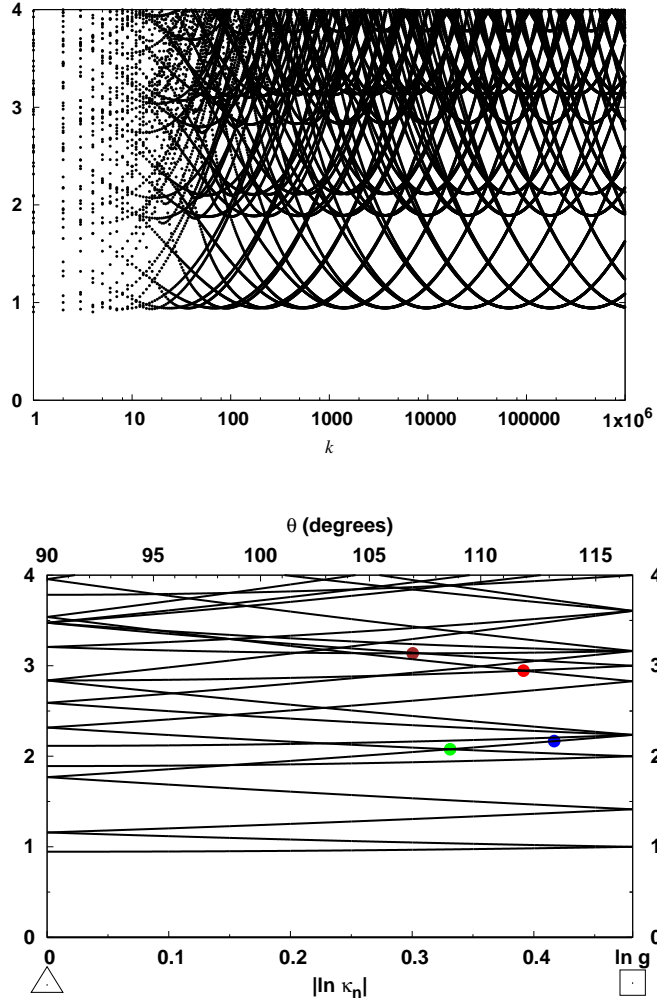
Figure 2: The top panel shows node k plotted against its distances to neighbouring points. As k increases this limits to a log-periodic repetition and reflection of the lower panel, which shows lattice distances for the general lattice between the isosceles (left) and square (right). Other special lattices and distances discussed throughout this paper are indicated by the coloured dots. The lower scale uses κ_n as in Eq. (20). The upper scale uses angle θ as in Eq. (24).

In other words, for any lattice vector defined by the integers (a, b), there is another vector $(-a + 2b, 2a + b)$ of magnitude exactly a factor $\sqrt{5}$ greater, and a further lattice vector $(b, a+b)$ at the midpoint of these. The set of such lattices (up to scale and orientation) forms a one parameter family, determined by the angle between one basis vector, say $(1, 0)$, and the vector of magnitude $\sqrt{5}$ greater, $(-1, 2)$. The midpoint $(0, 1)$ is the other basis vector. The angle θ between the vectors $(1, 0)$ and $(-1, 2)$, using Eqs. (16,17), satisfies

$$\cos\theta = \frac{g^{4n} - 80\pi^2 k^2}{g^{4n} + 80\pi^2 k^2} \tag{23}$$

which can be rearranged to give

$$k = \frac{g^{2n}}{4\pi\sqrt{5}} \tan\frac{\theta}{2} \tag{24}$$

from which we find that all such lattices appear in the sunflower spiral. In terms of κ_n defined above, we have $\kappa_n = \tan(\theta/2)$. The square lattice corresponds to $\theta = \arccos(-1/\sqrt{5}) = 2\arctan(g)$ and the isosceles lattice to $\theta = \pi/2$.

5 Delone properties and stretch factor

Numerically, the smallest separation distance between two points is found to be $d_{1,4} \approx 0.90380$. To prove this, one could note that the shortest distance of any lattice is $\sqrt{\frac{2}{\sqrt{5}}} \approx 0.945742$ (above), and then put quantitative bounds on the neglected $\mathcal{O}(1/\sqrt{k})$ terms, and test numerically as far as required for the bounds.

The fact there is a shortest distance means that the point set S is s-uniformly discrete, that is, each ball of radius s contains at most one point, for $s < d_{1,4}/2$. The set is also r-relatively dense, that is, each ball of radius r is non-empty, for $r > r_{rd} \approx 0.843859$, where this value corresponds to the (numerical) point $(0.48728, 0.06150)$ furthest from any point in the set and a distance r_{rd} from each of the points $k = 2, 3, 5$. Having both s-uniform discreteness and r-relative density, the set S is called a Delone set. It is also an ϵ-net, that is, $\epsilon/2$-uniformly discrete and ϵ-relatively dense [Cla06], for $r_{rd} < \epsilon < d_{1,4}$. See Ref. [Aki20] for proofs of the Delone property in the present model, for a general rotation number that is badly approximable by rationals (such as g).

The ϵ-net property relies on the above inequality and it is interesting to briefly consider the rotation numbers α for which this holds. Numerically, it is found to be true for $\alpha = (g + a)^{-1}$ for $a \in \{1, 2, 3\}$, where $a = 1$ gives $\alpha = g^{-2}$ which is equivalent to g studied here, since $g^{-2} = 2 - g$, adding 2 adds $4\pi k$ to ϕ_k and the minus sign gives a reflection across the x-axis. There are likely no other values of α with the ϵ-net property, but it is delicate since both r and $2s$ vary wildly with α, and can approach each other quite closely for many other values of α. We return to the main case studied here, of $\alpha = g$.

A general exposition of the above properties and application to generating triangulations on general curved spaces is given in Ref. [Cla06]. The relevant triangulation on $\mathbb{R}^2$, usually called the Delaunay triangulation (same mathematician as
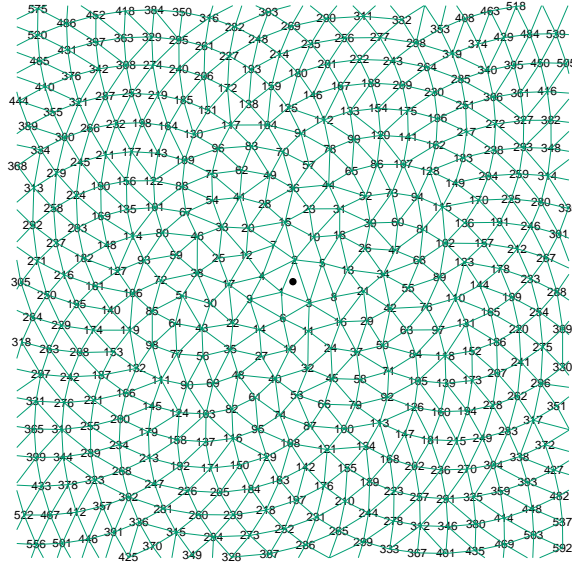
Figure 3: The Delaunay triangulation of S.

Delone, but spelt differently), can be defined as the union of triangles whose circumcircles contain no other points of S. See Fig. 3 here and Fig. 13b of Ref. [Mac21]. The Delaunay triangulation can be considered as a graph, however is not a hard disk graph, since it contains the link between $k = 3, 5$ of length 1.52674, but for a link formation distance $R > \sqrt{2}$ both diagonals exist at the square lattice, so the graph is not a triangulation.

Every Delaunay triangulation is known to have a stretch factor (also called spanning ratio), defined as the maximum ratio of the distances between two nodes along graph links and the Euclidean separation [Bos13], that is at most 1.998 [Xia11]. Numerically, the spanning ratio of the Delaunay triangulation of S is found to be $\sqrt{2}$, occurring at the square lattice. That is, each square has a single diagonal filled, but not both as it would violate planarity. Then, for the corners that at not linked, the ratio between the Euclidean separation ($\sqrt{2}$) and distance following graph links (2) is $\sqrt{2}$. Also, there are no other locations, even close to the origin, that have a greater stretch factor.

There are results for the spanning ratio of hard disk graphs as well [Bos13]. These depend on R, for example at $R = \sqrt{2}$ the diagonals of the square lattice appear, reducing the stretch factor there to $\sqrt{4 - 2\sqrt{2}} \approx 1.08239$. For $\sqrt{3/\sqrt{5}} \leq R < \sqrt{7/\sqrt{5}}$ the stretch factor of the isosceles lattice is $\sqrt{2(6 - \sqrt{6})/5} \approx 1.19172$. In general, the stretch factor of a lattice is shown to be $\sec(\vartheta/2)$ where ϑ is the maximum angle between adjacent vectors defined by the links.

The stretch factor of the hard disk graph of S is plotted in Fig. 4. It is difficult to obtain analytically, since it is dominated by nodes at small k for most R. Some

11
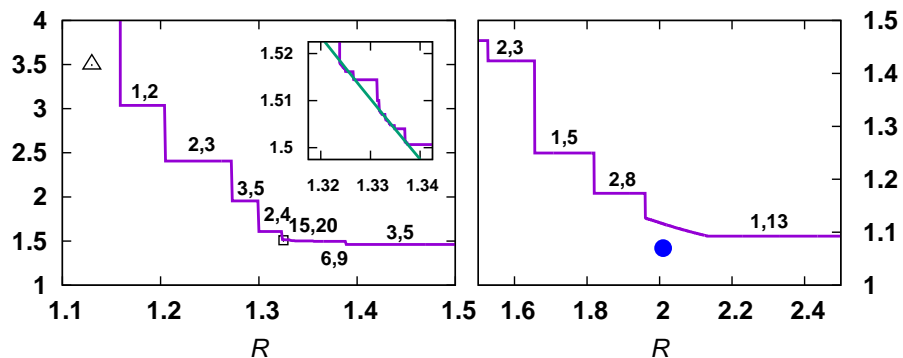
Figure 4: Stretch factor as a function of R, labelled by the location of the determining links, and isosceles and blue lattices as in Fig. 2. The left and right panels give different regions with different scales on the axes. The inset shows a region where there are many distant points, where the graph is close to adding the short diagonal of approximate parallelograms, together with a curve giving a lower bound from the lattices at infinity. The numerical simulation uses data for $k \leq 10000$.

exceptions are as follows: For $1 < R < \sqrt{3/\sqrt{5}} \approx 1.15829$ the graph is connected but near the isosceles lattice is composed of parallel lines, leading to infinite stretch factor. There are some values near $R \approx 1.33$ where the stretch factor is controlled by the location where the short diagonal of a parallelogram first appears; see the inset in Fig. 4. Finally, for $1.96066 \approx d_{2,8} < R \lesssim 2.16729$ there are some lattices (different from but close to the square lattice) which have a stretch factor greater than 1.09248 which is the stretch factor associated with the link $1, 13$ for slightly larger R. The limiting such lattice is shown by the blue dot in Fig. 2.

6 Forming links, connectivity and planarity

Let us now consider the transitions of the hard disk graph on S as a function of the connection range R. As with the previous sections, we first consider the large

(a,b)	$\left\|\frac{a+gb}{a-b/g}\right\|$	$a^2 + ab - b^2$	$\delta^*_{a,b}$
(1,0)	1	1	0.94574
(2,0)	1	4	1.89148
(2,1)	g^2	5	2.11474
(3,0)	1	9	2.83722
(3,1)	$\frac{10+7g}{11}$	11	3.13667
(4,0)	1	16	3.78297
(4,1)	$\frac{17+9g}{19}$	19	4.12239
(4,2)	g^2	20	4.22949
(5,0)	1	25	4.72871

Table 1: Link formation transitions. See Eq. (25) and following.

k behaviour, that is, the properties of the graph far from the origin. The general lattice vector corresponding to the displacement from k to $k + aF_n + bF_{n+1}$ is given in Eqs. (16) and (17) above.

First, we discuss link formation transitions. The squared distance $\delta^2_{a,b} = \xi^2 + \eta^2$ is minimised at

$$k^*_{a,b} = \frac{g^{2n}}{4\pi\sqrt{5}} \left| \frac{a + gb}{a - b/g} \right| \tag{25}$$

and is given by

$$\delta^*_{a,b} = \sqrt{\frac{2}{\sqrt{5}} |a^2 + ab - b^2|} \tag{26}$$

which is independent of n. Therefore, as R increases above $\delta^*_{a,b}$ these vectors that connect k and $k + aF_n + bF_{n+1}$ form links and are added to the hard disk graph. As seen in Fig. 5, these links appear at concentric circles in the lattice corresponding to different values of n, which then expand into annuli.

The link formation transitions are given in Tab. 1 and are visible in Fig. 2 as the lowest points of the distance curves. Many lattice vectors (a,b) are equivalent under translation by n, and so are not given separately in the table. For example the first transition is at $(1,0)$ corresponding to F_n. The transition $(0,1)$ is F_{n+1}, so it is the same transition, obtained by shifting n by one. Likewise $(1,1)$ is $F_n + F_{n+1} = F_{n+2}$ is the same transition shifting n by two. Many of the transitions that are distinct are however located at the isosceles lattice, where $\frac{a+gb}{a-b/g}$ is an even power of g, so $k^*_{a,b}$ is of the form $\frac{g^{2n}}{4\pi\sqrt{5}}$.

The first non-isosceles transition at $R = \delta^*_{3,1} = 3.13667$ is indicated by the brown dot in Fig. 2, corresponding to the lowest point of the relevant curve. It is the lattice where $(2, -3)$ and $(1, 4)$ have the same length. The lattice generated by these vectors is however a scaled isosceles lattice.

At finite k, numerical investigations indicate that the initial transition $(1,0)$ is well described by Eqs. (25,26), with the shortest link at each isosceles lattice between values of k equal to or within one of $\frac{g^{2n}}{4\pi\sqrt{5}} \pm \frac{g^n}{2\sqrt{5}}$ with the second term giving the Fibonacci number. Due to the distortion of the lattice, this shortest
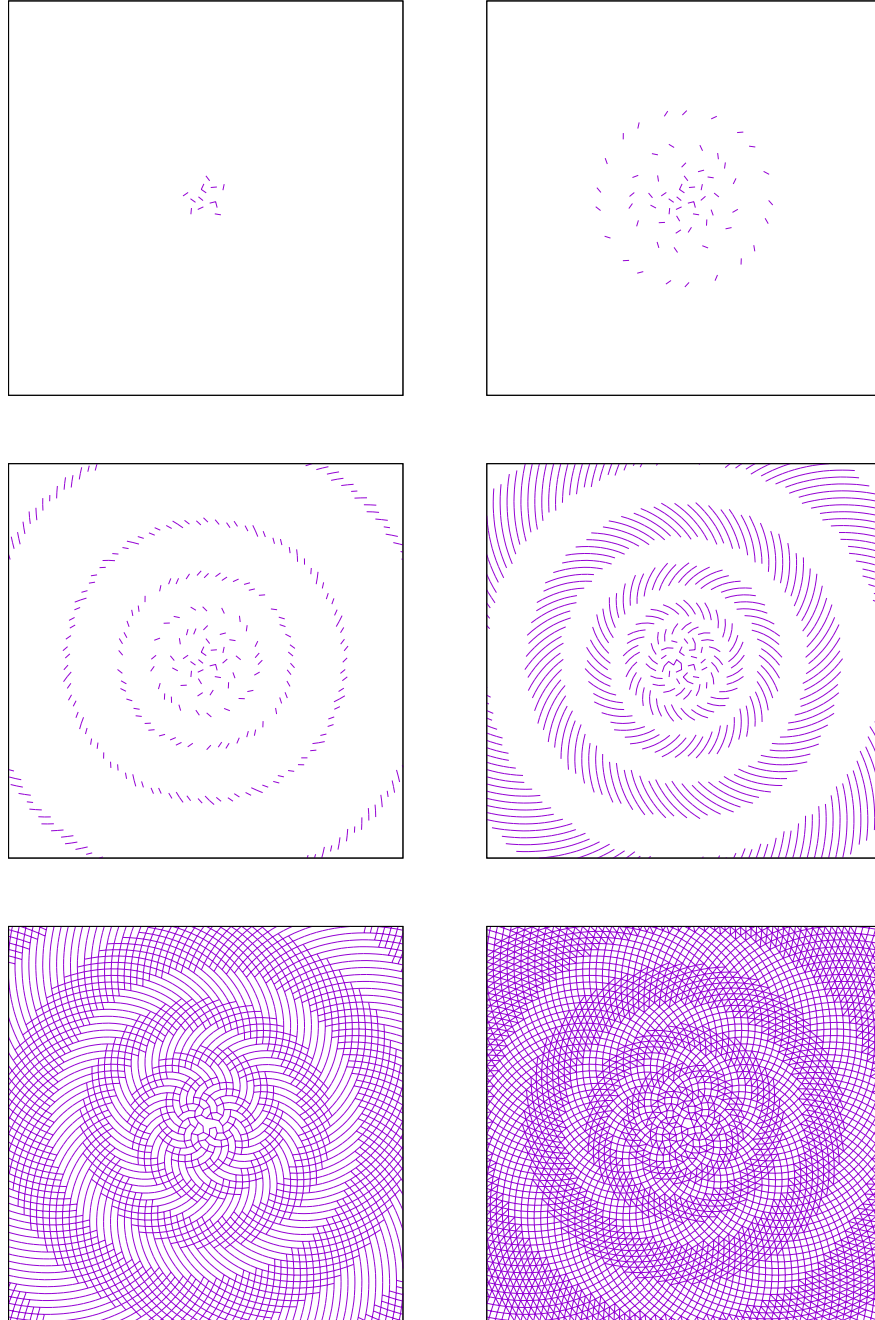
Figure 5: The first link formation transition at $R = \sqrt{2/\sqrt{5}} \approx 0.94574$. The plotted hard disk graphs are 0.944 (upper left), 0.9456 (upper right), 0.946 (middle left) and 0.96 (middle right). As R increases further, the lines of links extend further and cross. The lower plots are for 1.08 (lower left) and 1.3 (lower right).
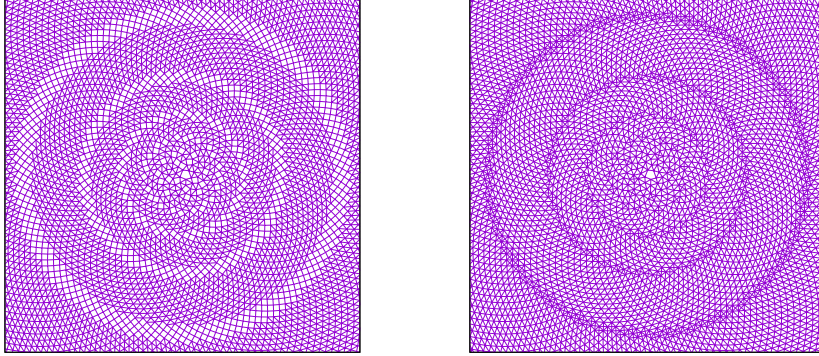
Figure 6: Planarity transition at $R = \sqrt{2} \approx 1.41421$. The plotted hard disk graphs are 1.35 (left) and 1.45 (right).

link is shorter than the limiting value of $\delta_{1,0}^* = \sqrt{2/\sqrt{5}}$, thus the transitions move outwards to larger n as this value is approached from below. This is visible in Fig. 5.

There are (at least) two transitions of a different kind, that occur at the square lattice. Inspection of Figs. 2 and 5 shows that the links formed at the initial $(1,0)$ link formation transition move inward and outward, and touch around $R = 1$ at the square lattice, before continuing smoothly to form the equivalent links $((0,1)$ and $(-1,1))$ in neighbouring annuli. As soon as $R > 1$, the whole network connects (for large k, and numerically all nodes are connected to large k). Similarly, when $R > \sqrt{2}$ they have reached the square lattice again, forming the diagonals of the squares, and hence making the graph nonplanar. See Fig. 6. Numerically, $R = 1$ does not connect (see Fig. 1), and $R = \sqrt{2}$ is planar. Note that here, percolation (defined as the existence of an infinite cluster) and connectivity occur at the same value $R = 1$, though exactly at the transition point there appear to be multiple infinite clusters.

7   Node degrees

The graph is infinite and care is needed in defining the degree distribution. Arguably the most natural, given the log-periodicity in k of the lattices, uses logarithmic averaging, which gives the probability mass function

$$p_D = \lim_{K \to \infty} \frac{1}{\ln K} \sum_{k=1}^{K} \frac{1}{k} \mathbf{1}_{d_k = D} \tag{27}$$

15
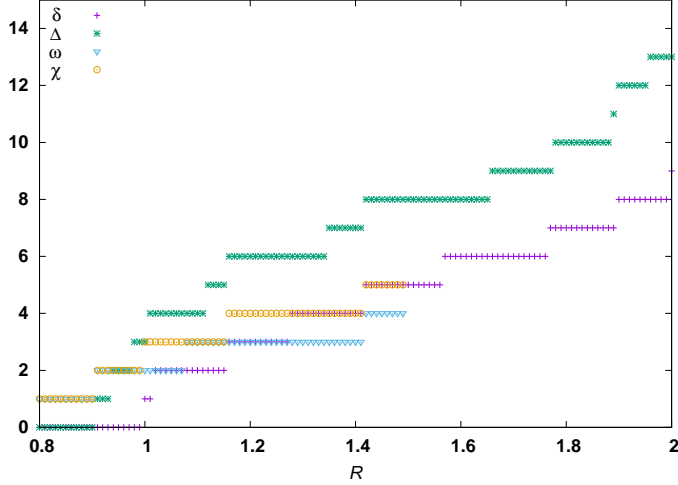
Figure 7: Minimum and maximum degrees, and clique and chromatic numbers, as presented in Sections 7 and 8.

where p_D is the probability (in this sense) of a node having degree D, and $\mathbf{1}_{d_k=D}$ is the characteristic function equal to one if node k has degree D and zero otherwise. Then, the mean degree is $\bar{D} = \sum_{D=0}^{\infty} D p_D$, a finite sum. It is possible in principle to calculate p_D for a fixed R, by determining which large k lead to lattices where nodes have each degree, but we have not done this. Small k effects are not relevant since they are are finite, and divided by $\ln K$.

It is however simpler to consider the minimum degree δ and maximum degree Δ, which are defined and monotonically increasing as a function of R; see Fig. 7. Practically all the claims in this section are numerical, though there are some related rigorous results in [Aki20], including for rotation numbers other than g.

The transitions $R = R_*$ at which δ and Δ increase are broadly of two kinds. The first kind occurs at finite k, in which case we have some j, k so that $d_{j,k} = R_*$ and one of these nodes (say, j) has the minimum degree for $R_* - \epsilon < R < R_*$ or the maximum degree for $R_* \leq R < R_* + \epsilon$. The parameter δ or Δ changes by one, since all distances in the sunflower spiral are distinct (presumably, but hard to prove). The second kind occurs at infinity, in which case there is an increasing sequence of j with minimum degree for $R_* - \epsilon < R < R_*$ or maximum degree for $R_* < R < R_* + \epsilon$ (note the different inequality). The sequences are located at particular (square or isosceles or other) lattices, and the transition point R_* is related to a lattice with two distances nontrivially equal to R_*, and so it is an algebraic number. In this case δ or Δ may change by more than one, at least numerically; examples are given below.

These transitions are plotted in Fig. 8, with k limited to 10^6. There are many finite transitions, including some observable patterns, which we will not attempt

16
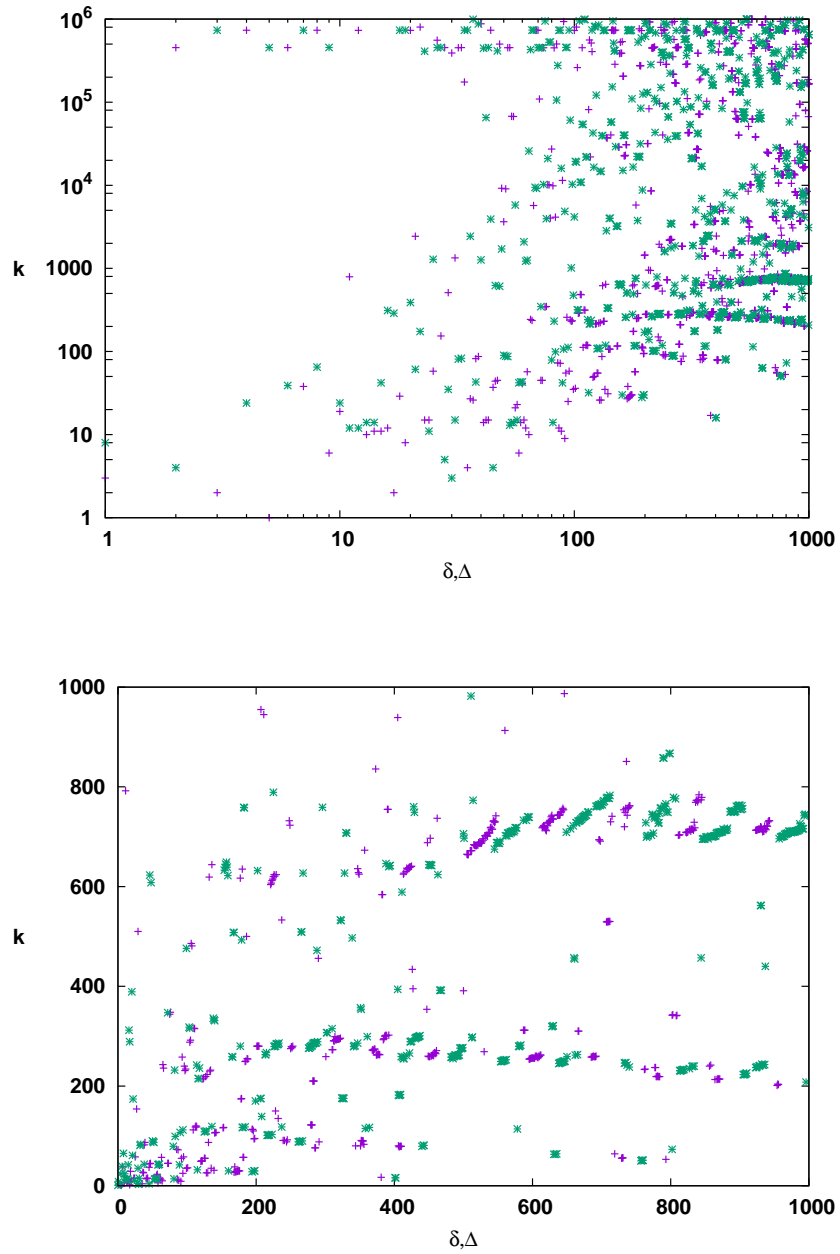
Figure 8: Transitions in minimum degree δ (purple plusses) and maximum degree Δ (green stars), occurring when R is varied. The vertical axis gives the value of k at which the relevant link occurs, for $k \leq 10^6$. The upper panel has a log scale and the lower panel is linear.

	δ			Δ		
Degree	k	R_*	Numerical	k	R_*	Numerical
1	$\square$	1	1.00000	1,4	$d_{1,4}$	0.90380
2	3	$d_{3,11}$	1.01052	8	$d_{8,16}$	0.93485
3	$\triangle$	$\sqrt{3/\sqrt{5}}$	1.15829	4	$d_{4,12}$	0.97466
4	2	$d_{2,1}$	1.27232	$\square$	1	1.00000
5	$\square$	$\sqrt{2}$	1.41421	24	$d_{24,32}$	1.11953
6	1	$d_{1,14}$	1.56467	$\triangle$	$\sqrt{3/\sqrt{5}}$	1.15829
7	$\triangle$	$\sqrt{7/\sqrt{5}}$	1.76932	39	$d_{39,73}$	1.34104
8	38	$d_{38,12}$	1.89065	$\square$	$\sqrt{2}$	1.41421
9	$\square$	2	2.00000	65	$d_{65,120}$	1.65407
10	6	$d_{6,8}$	2.01761	$\triangle$	$\sqrt{7/\sqrt{5}}$	1.76932

Table 2: Transitions in minimum and maximum degree. The $\square$ and $\triangle$ refer to transitions at infinity at the square and isosceles lattices respectively.

to explain in detail except to note that in the lower panel of Fig. 8 the lines of alternating δ and Δ transitions are approximately affinely related, scaled by a factor g in the horizontal direction and g^2 in the vertical direction. For the infinite transitions, we can see many at the square lattice at $k = \frac{g^{35}}{4\pi\sqrt{5}} \approx 734298$ and the isosceles lattice at $k = \frac{g^{34}}{4\pi\sqrt{5}} \approx 453821$.

The first few degree transitions are also presented in Tab. 2. Note that at distances found in the square and isosceles lattices, there are often transitions occurring simultaneously in both minimum and maximum degree. There are clusters of values where $k \approx \Delta$, for example $k \in [\Delta-1, \Delta+1]$ for $\Delta = 12, 13, 14, 15$ and for eleven values in $\Delta \in [277, 290]$; here the connection range is sensing the non-lattice region near the origin.

The first degree that is skipped is $\Delta = 19$; for $R = \sqrt{5}$ we have $\Delta = 18$ (at least to $k = 10^6$), whilst just above this value the square lattice at infinity gives $\Delta = 20$. Similarly $\delta = 33$ is apparently skipped at the isosceles lattice length $\sqrt{27/\sqrt{5}} \approx 3.47488$. In both instances, these are the smallest lengths at which eight points in the lattice are equidistant from the origin.

The first lattice at infinity that is not square or isosceles is at $\delta = 23$. This corresponds to a unit covolume lattice for which the vectors $(2, 2)$ and $(3, 0)$ have the same length, equal to $R_* = (11664/155)^{1/4} \approx 2.94530$ and found at $k = \frac{6\sqrt{5}-5}{\sqrt{31}}\frac{g^{2n}}{4\pi}$. It is shown as the red dot in Fig. 2.

We note that it is possible to consider asymptotic minimum and maximum degrees δ_∞ and Δ_∞, which consider only the lattices at infinity and ignore a finite number of links near the origin. For almost all R, the asymptotic degree for each lattice may be read off the lower panel of Fig 2 noting that each curve corresponds to a degree of two due to symmetry. So, for example, when $\sqrt{3/\sqrt{5}} < R < \sqrt{2}$

we consider a horizontal line at that height and its intersection with the curve. Lattices on the left, near the isosceles lattice, have degree six, whilst lattices on the right, near the square lattice, have degree four. Values of R corresponding to exact distances of the isosceles or square lattices, or for larger values, where the curves intersect, correspond to transitions in the asymptotic degrees. Exactly at the transition a more careful analysis is needed. For example, at $R = 1$, the square lattice goes from degree zero to degree four. Inspection of Fig. 1 shows that most nodes have degree two, but there are nodes of degree one and three far from the origin.

It can also be seen from Fig 2 that all lattices, except the one at the transition, have the same degree, for the values $R \in \{1, \sqrt{3/\sqrt{5}} \approx 1.15829, \sqrt{2} \approx 1.41421, \sqrt{7/\sqrt{5}} \approx 1.76932, 8/220^{1/4} \approx 2.07723\}$ where the last is shown by the green dot in Fig. 2 and is not in either isosceles or square lattices. It is near the square lattice, but with vectors $(-2, 1)$ and $(0, 2)$ of equal length.

Finally, another asymptotic limit is that of $R \to \infty$. Since there is unit density, we have $\delta \sim \Delta \sim \pi R^2$. It would be interesting, but is beyond the scope of this work, to analyse the range of degrees $\Delta - \delta$, derived from the family of lattices appearing here, in comparison with a single lattice (where $\Delta - \delta = 0$), low discrepancy graphs [Est17] and RGG on a torus (where the degree distribution is Poisson). This seems related to the (very difficult) Gauss circle problem [Hux02].

8   Clique and chromatic numbers

The clique number ω and chromatic number χ of a graph are bounded as follows:

$$\omega \leq \chi \leq \Delta \tag{28}$$

except where the graph has a connected component that is complete or an odd cycle where we can have $\chi = \Delta + 1$. The latter happens here only when $R < d_{8,16} \approx 0.93485$; above this the node $k = 8$ has degree 2, but there are no K_3 or larger complete graphs or odd cycles formed before $R > 1$ when the whole graph is connected.

Finding the largest cliques and chromatic number is in general a hard problem, even taking into account some simplifications that come from the geometry. The structure of the transitions is likely to be similar to that of the minimum and maximum degrees.

Results for the clique number about which we have good numerical evidence are:

$$\omega = \begin{cases} 1 & R < d_{1,4} \approx 0.90380 \\ 2 & d_{1,4} \leq R < d_{2,10} \approx 1.07024 \\ 3 & d_{2,10} \leq R \leq \sqrt{2} \approx 1.41421 \\ \geq 4 & \sqrt{2} < R \end{cases} \tag{29}$$

Here, the first link is $k = \{1, 4\}$, the first triangle is $k = \{2, 5, 10\}$ and the first tetrahedron K_4 is where both diagonals are formed in the square lattice at large distances.
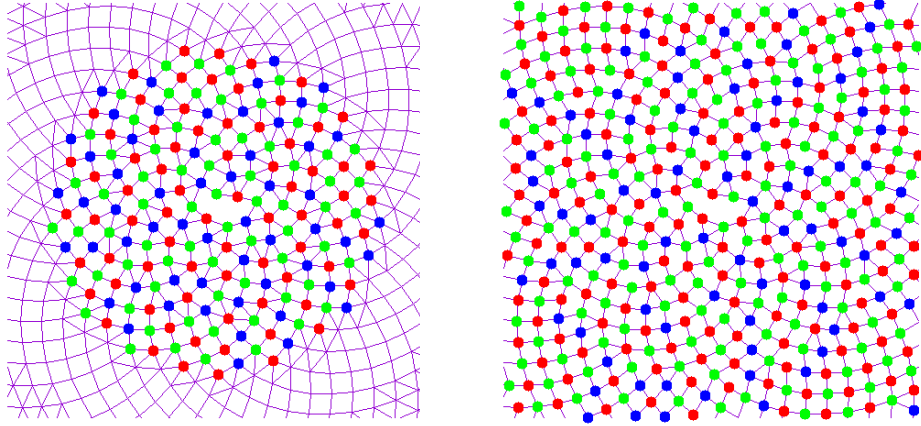
Figure 9: 3-colourings of the sunflower graph. Left: $k \leq 200$ and $R = 1.247 \lesssim d_{89,102}$. Right: $k \leq 1000$ and $R = 1.158 \lesssim \sqrt{3/\sqrt{5}}$.

Similarly, we are reasonably confident about the following results for the chromatic number:

$$\chi = \begin{cases} 1 & R < d_{1,4} \approx 0.90380 \\ 2 & d_{1,4} \leq R \leq 1 \\ 3 & 1 < R \leq \sqrt{3/\sqrt{5}} \approx 1.15829 \\ 4 & \sqrt{3/\sqrt{5}} < R \leq \sqrt{2} \approx 1.41421 \\ \geq 5 & \sqrt{2} < R \end{cases} \tag{30}$$

Here, $\chi \geq 3$ where the cycles (including odd cycles) appear. While the graph remains planar, we must have $\chi \leq 4$ due to the four colour map theorem. A square lattice with diagonals has $\chi = 4$, but when this is formed for $R > \sqrt{2}$, there are perturbations, in particular forming it in annuli at large distance, almost certainly requiring $\chi \geq 5$.

The above does not show where the transition between $\chi = 3$ and $\chi = 4$ occurs. We have done numerical simulations which either find a 3-colouring, prove that one does not exist, or (for $k \gtrsim 200$) take an exponentially long time to decide. Fig. 9 shows a 3-colouring for $k \leq 200$ and $R = 1.247 \lesssim d_{89,102}$, which is the limit for this k. But it is clear that this colouring cannot be continued to larger k. The true boundary appears to be $R = \sqrt{3/\sqrt{5}} \approx 1.15829$ at which triangles appear in the isosceles lattice at large distances. At this value, the colouring easily continues to at least $k = 10^5$. These values of ω and χ, together with δ and Δ from the previous section, are plotted in Fig. 7.

At large R we expect that all degrees are of order the area of the disk of radius R, so $\delta, \Delta \sim \pi R^2 \approx 3.142R^2$. In contrast, cliques are of order the area of the disk of diameter R, so $\omega \sim \pi R^2/4 \approx 0.785R^2$. For chromatic numbers, we expect that

20

the result is as given by a tiling of the plane with hexagons of lattice vector R, and the nodes within each hexagon having distinct colours. This is similar to the dense regime of the random geometric graph [McD03], and gives $\chi \sim \sqrt{3}R^2/2 \approx 0.866R^2$ which is close to, but above, the ω value.

9   Conclusion

Here we considered the sunflower spiral, its Delone properties and its hard disk graph of the sunflower spiral as a function of the link range R, finding a rich and varied structure, much of which is accessible analytically. Some properties, such as stretch factor, are mostly determined by local structure near the origin, however even here there is a region near $R = 1.33$ where there is intricate detail from distant regions (see Fig. 4). The link formation, connectivity and planarity transitions are accessible analytically (see Sec. 6) but minimum and maximum degrees are controlled either by local or distant regions. Even where the transitions are related to distant lattices, properties exactly at the relevant R value, and for the chromatic number, depend sensitively on the small perturbations of these lattices at large distances.

There is a huge variety of open problems and possible future directions, including a more detailed study of the above graphs and properties, more global properties such as shortest paths and graph spectra, other deterministic graphs on the sunflower spiral (for example annulus rather than disk, k-nearest neighbour, beta-skeleton), random graphs on the sunflower spiral (for example percolation, soft random geometric graph [Det16]). Then, there are similar point sets derived from other irrational numbers, whose Diophantine properties are likewise described using their continued fraction expansions. Finally, we can consider higher dimensional generalisations, for example as discussed in Ref. [Adi22a].

References

[Adi22a] F. Adiceam and I. Tsokanos, "Higher dimensional spiral Delone sets," Functiones et Approximatio Commentarii Mathematici **67**, 21–46 (2022).

[Adi22b] F. Adiceam and I. Tsokanos, "Visibility properties of spiral sets," Moscow Journal of Combinatorics and Number Theory **11**, 149–159 (2022).

[Aki20] S. Akiyama, "Spiral Delone sets and three distance theorem," Nonlinearity **33**, 2533–2540 (2020).

[Bar11] M. Barthélemy, "Spatial networks," Physics Reports **499**, 1–101 (2011).

[Bar16] J. Barberena, A. M. Larrayoz, M. Sánchez and A. Bernardos, "State-of-the-art of heliostat field layout algorithms and their comparison," Energy Procedia **93**, 31–38 (2016).

[Bos13] P. Bose and M. Smid, "On plane geometric spanners: A survey and open problems," Computational Geometry **46**, 818–830 (2013).

[Cla06] K. L. Clarkson, "Building triangulations using ε-nets," in *Proceedings of the thirty-eighth annual ACM symposium on Theory of computing*, 326–335 (2006).

[Det16] C. P. Dettmann and O. Georgiou, "Random geometric graphs with general connection functions," Physical Review E **93**, 032313 (2016).

[Det18] C. P. Dettmann, O. Georgiou and P. Pratt, "Spatial networks with wireless applications," Comptes Rendus Physique **19**, 187–204 (2018).

[Dou92] S. Douady and Y. Couder, "Phyllotaxis as a physical self-organized growth process," Phys. Rev. Lett. **68**, 2098–2101 (1992).

[Est15] E. Estrada and P. A. Knight, *A first course in network theory* (Oxford University Press, USA, 2015).

[Est17] E. Estrada, "Quasirandom geometric networks from low-discrepancy sequences," Physical Review E **96**, 022314 (2017).

[Gor18] S. Gorsky, R. Zhang, A. Gok, R. Wang, K. Kebede, A. Lenef, M. Raukas and L. Dal Negro, "Directional light emission enhancement from led-phosphor converters using dielectric vogel spiral arrays," APL Photonics **3**, 126103 (2018).

[Hux02] M. N. Huxley, "Integer points, exponential sums and the riemann zeta function," in *Surveys in Number Theory*, 109–124 (AK Peters/CRC Press, 2002).

[Las18] G. Last and M. Penrose, *Lectures on the Poisson process* (Cambridge University Press, 2018).

[Law13] J. D. Lawrence, *A catalog of special plane curves* (Courier Corporation, 2013).

[Lek51] C. G. Lekkerkerker, "Voorstelling van natuurlijke getallen door een som van getallen van fibonacci," Stichting Mathematisch Centrum. Zuivere Wiskunde (1951).

[Mac21] E. Maciá, "Aperiodic crystals in biology," Journal of Physics: Condensed Matter (2021).

[Mar20] J. Marklof, "Delone sets generated by square roots," The American Mathematical Monthly **127**, 836–840 (2020).

[McD03] C. McDiarmid, "Random channel assignment in the plane," Random Structures & Algorithms **22**, 187–212 (2003).

[Men23] L. Meng, J. Zhang, Y. Hou, P. Breitkopf, J. Zhu and W. Zhang, "Revisiting the fibonacci spiral pattern for stiffening rib design," International Journal of Mechanical Sciences 108131 (2023).

[Ost22] A. Ostrowski, "Bemerkungen zur theorie der diophantischen approximationen," in *Abhandlungen aus dem Mathematischen Seminar der Universität Hamburg*, volume 1, 77–98 (Springer, 1922).

[Pen16] M. D. Penrose, "Connectivity of soft random geometric graphs," The Annals of Applied Probability **26**, 986–1028 (2016).

[Pri18] A. Price and B. Long, "Fibonacci spiral arranged ultrasound phased array for mid-air haptics," in *2018 IEEE International Ultrasonics Symposium (IUS)*, 1–4 (IEEE, 2018).

[Roc92] A. M. Rockett and P. Szüsz, *Continued fractions* (World Scientific, Singapore, 1992).

[Spe18] L. Speidel, H. A. Harrington, S. J. Chapman and M. A. Porter, "Topological data analysis of continuum percolation with disks," Physical Review E **98**, 012318 (2018).

[Tre12] J. Trevino, S. F. Liew, H. Noh, H. Cao and L. Dal Negro, "Geometrical structure, multifractal spectra and localized optical modes of aperiodic vogel spirals," Optics express **20**, 3015–3033 (2012).

[Tro21] O. J. Trojak, S. Gorsky, C. Murray, F. Sgrignuoli, F. A. Pinheiro, L. Dal Negro and L. Sapienza, "Cavity-enhanced light–matter interaction in vogel-spiral devices as a platform for quantum photonics," Applied Physics Letters **118**, 011103 (2021).

[Vog79] H. Vogel, "A better way to construct the sunflower head," Mathematical biosciences **44**, 179–189 (1979).

[Wal11] M. Walters, "Random geometric graphs," Surveys in Combinatorics **392**, 365–402 (2011).

[Xia11] G. Xia, "Improved upper bound on the stretch factor of Delaunay triangulations," in *Proceedings of the twenty-seventh annual symposium on Computational geometry*, 264–273 (ACM, 2011).

[Yam20] Y. Yamagishi, "Spiral Delone sets in relative metric," arXiv preprint arXiv:2012.07282 (2020).

[Yam21] Y. Yamagishi, T. Sushida and J.-F. Sadoc, "Area convergence of Voronoi cells on spiral lattices," Nonlinearity **34**, 3163–3183 (2021).